

# Cosmic String Loop Collapse in Full General Relativity

Thomas Helfer<sup>a,\*</sup>, Josu C. Aurrekoetxea<sup>a,†</sup> and Eugene A. Lim<sup>a,‡</sup>  
<sup>a</sup>*Theoretical Particle Physics and Cosmology Group, Physics Department,  
 Kings College London, Strand, London WC2R 2LS, United Kingdom*

We present the first fully general relativistic dynamical simulations of Abelian-Higgs cosmic strings using 3+1D numerical relativity. Focusing on cosmic string loops, we show that they collapse due to their tension and can either (i) unwind and disperse or (ii) form a black hole, depending on their tension  $G\mu$  and initial radius. We show that these results can be predicted using an approximate formula derived using the hoop conjecture, and argue that it is independent of field interactions. We extract the gravitational waveform produced in the black hole formation case and show that it is dominated by the  $l = 2$  and  $m = 0$  mode. We also compute the total gravitational wave energy emitted during such a collapse, being  $0.5 \pm 0.2$  % of the initial total cosmic string loop mass, for a string tension of  $G\mu = 1.6 \times 10^{-2}$  and radius  $R = 100 M_{\text{Pl}}^{-1}$ . Extrapolating these results to the current bound of  $G\mu \sim 10^{-8}$ , we forecast that such events could be detected by LIGO/VIRGO at about once per decade and hundreds per year by the Einstein Telescope.

## I. INTRODUCTION

The recent detection of Gravitational Waves (GW) from black hole [1] binaries by the LIGO/VIRGO collaboration marked the start of a new era of observations. Beyond astrophysical objects such as black holes and neutron stars, this paved the way for the use of GW to search directly for signatures of new physics. One of the key targets for this search are cosmic strings [2–4].

Cosmologically, cosmic strings networks naturally arise after a phase transition in the early universe, possibly during GUT symmetry breaking. More speculatively, string theory also suggests the presence of cosmological fundamental superstrings, especially through the mechanism of brane inflation [5, 6]. These networks may manifest themselves through several channels, such as imprints via lensing on the Cosmic Microwave Background [7] and possibly through the presence of a stochastic gravitational wave background. The latter in particular is recently searched for by the LIGO/VIRGO collaboration [3]. More intriguingly, one can search for localized coherent events of these strings, such as when the strings self-interact through the formation of sharp cusps or through the collisions of traveling kinks that are formed during the intercommutation (i.e. collisions) of cosmic strings.

Before this work, the two primary methods of modeling cosmic strings has been through solving the field theory equations in flat or expanding spacetime, or through an effective Nambu-Goto prescription with weak coupling to gravity (see e.g. [8]). In either case, by considering the stress-energy of a network of strings, one can then compute in the weak gravity limit a stochastic GW background [9, 10]. Local events such as the collisions of traveling kinks and cusps along the strings are expected

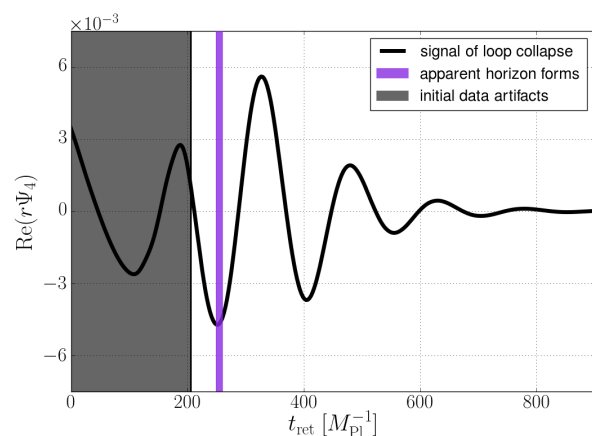


FIG. 1. **GW for a black hole formed from circular cosmic string loop collapse:** We plot the real part of the dominant  $l = 2$   $m = 0$  mode of  $r\Psi_4$  over time. The loop has tension  $G\mu = 1.6 \times 10^{-2}$  and an initial radius  $R = 100 M_{\text{Pl}}^{-1}$ . The grey shaded area of the plot are mixed with stray GWs that arise as artifacts of the initial data. The x-axis  $t_{\text{ret}} = t - r_{\text{ext}}$  is the retarded time where  $r_{\text{ext}}$  is the extraction radius.

to produce bursts of GW – these bursts events have been computed using the Nambu-Goto approximation, again in the weak field limit [10]. These two methods do not coincide in general, mainly due to their disagreement on the primary energy loss mechanism of the cosmic strings (see [11–16]).

Going beyond the weak field limit requires the finding of the solutions to the full field theory coupled to general relativity – and in this work we present the *first numerical relativity simulation of Abelian-Higgs cosmic strings in full general relativity*. In this first paper of a series, we numerically explore the collapse of a circular cosmic string loop in extreme regimes ( $4 \times 10^{-3} < G\mu < 4 \times 10^{-2}$ ). We show that whether the loop collapses into a black hole or unwinds itself depends on a simple analytic re-

\* thomashelfer@live.de

† j.c.aurrekoetxea@gmail.com

‡ eugene.a.lim@gmail.com

lation derived using the hoop conjecture. In the former case, we computed both the gravitational waveform (fig. 1) and its integrated GW energy emitted from such a collapse. For the latter, we found that the total energy emitted in gravitational waves is  $0.5 \pm 0.2$  % of the initial mass, which is in agreement with the Hawking bound of  $< 29\%$  [17]. We computed forecasts for possible detection with LIGO/VIRGO and the Einstein Telescope, which suggests that the former detect see up to an event per decade.

## II. ABELIAN-HIGGS WITH GRAVITY

The action of the Abelian Higgs model minimally coupled to gravity <sup>1</sup>

$$S = S_{EH} - \int d^4x \sqrt{-g} \left[ (D_\mu \phi)^* (D^\mu \phi) + \frac{1}{4} F_{\mu\nu} F^{\mu\nu} + V(\phi) \right], \quad (1)$$

where  $S_{EH} = \int d^4x \sqrt{-g} (R/16\pi G)$ ,  $D_\mu$  is the covariant derivative ( $\partial_\mu - ieA_\mu$ ) with its  $U(1)$  gauge field  $A^\mu$ , and  $V(\phi)$  is the potential of the complex scalar field  $\phi$  given by

$$V(\phi) = \frac{1}{4} \lambda \left( |\phi|^2 - \eta^2 \right)^2, \quad F_{\mu\nu} = \partial_\mu A_\nu - \partial_\nu A_\mu. \quad (2)$$

For simplicity, we set the charge  $e$  and the dimensionless coupling constant  $\lambda$  to obey the critical coupling limit

$$\beta = \frac{\lambda}{2e^2} = 1, \quad (3)$$

in which the Higgs and vector masses are identical and  $\mu$  simplifies to

$$\mu = 2\pi\eta^2. \quad (4)$$

As a check of our code, we numerically construct a fully relativistic infinite static string coupled to gravity and demonstrate that its evolution is indeed static and stable. The details of this construction can be found in the Supplementary Material.

In this paper, we consider circular string loops. To construct the initial conditions, we define toroidal coordinates

$$\begin{aligned} x &= \cos \theta (R + r \cos \varphi), \\ y &= \sin \theta (R + r \cos \varphi), \\ z &= r \sin \varphi, \end{aligned} \quad (5)$$

where  $R$  is the radius of the loop and choose the following ansatz for the field variables

$$\phi = f(r) e^{in\theta}, \quad A_\theta = \frac{n\alpha(r)}{e}, \quad (6)$$

where  $n$  is the winding number of the string which is set to one throughout this paper. To construct the loop we use the profile  $f(r)$  from the static string<sup>2</sup>. After making the conformal metric ansatz

$$\gamma_{ij} dx^i dx^j = \chi(dx^2 + dy^2 + dz^2), \quad (7)$$

we solve the Hamiltonian constraint to obtain the conformal factor  $\chi$ .

## III. RESULTS

We simulate the collapse of circular loops, scanning through the initial condition parameter radius  $R$  and the model symmetry-breaking scale  $\eta$  (and hence string tension via eq. 4), in the critical coupling limit with  $e = 1$  and  $\lambda = 2$ . The loop begins at rest but quickly accelerates to close to the speed of light due mainly to the string tension. We find this motion to be consistent with the Nambu-Goto action dynamics (see Supplementary Material)

$$r = R \cos \frac{\tau}{R}, \quad (8)$$

up to  $r \sim \delta$  which is the thickness of the string given by

$$\delta = \frac{1}{\eta\sqrt{\lambda}}, \quad (9)$$

and  $\tau$  is the time coordinate at spatial infinity. Depending on the choice of  $\mu$  and  $R$ , there are two possible outcomes: (i) the string unwinds itself and the resulting radiation disperses or (ii) a black hole forms.

This result can be predicted using the hoop conjecture as follows. A black hole forms if the loop mass  $M_{\text{loop}} = 2\pi\mu R$  is enclosed within a radius smaller than its Schwarzschild radius  $2GM_{\text{loop}}$ . In addition, the smallest volume in which a loop can be contained before the string unwinds has radius  $\delta$ , which sets the Schwarzschild radius the lower bound for black hole formation to be  $2GM_{\text{loop}} > \delta$ , or

$$R > \sqrt{\frac{1}{8\pi\lambda}} (G\mu)^{-3/2} M_{\text{Pl}}^{-1}. \quad (10)$$

Moreover, as the minimum radius of a loop is  $R = \delta$ , we don't expect dispersion cases for  $G\mu > (4\pi)^{-1}$  and all loops will form black holes. We find this estimate to be a good predictor (see fig. 2), which suggests that black hole formation is broadly independent of field interactions.

If a black hole forms, the amount of initial mass that falls into the black hole depends on the initial radius  $R$  for fixed  $G\mu$ , with the rest being radiated in either gravitational waves or matter.

<sup>1</sup> We use the  $-+++$  convention for the metric, and set  $\hbar = c = 1$  and  $M_{\text{Pl}} = 1/\sqrt{G}$ .

<sup>2</sup> See the Supplementary Material for details.

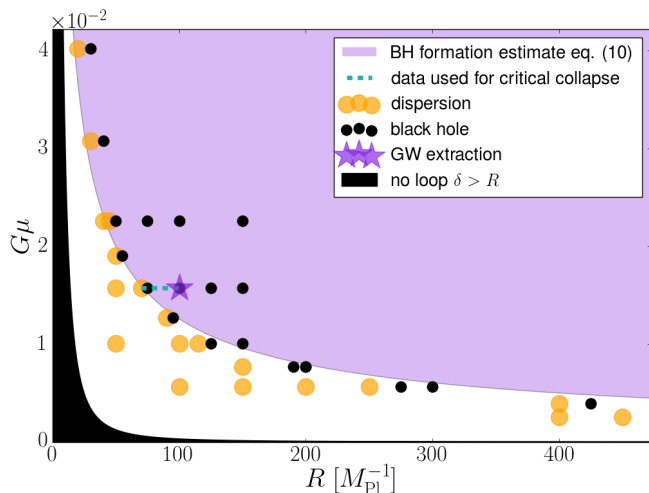


FIG. 2. **Overview of simulations** : The loop can either form a black hole or unwind and radiate all its mass. The analytical expression derived from the hoop conjecture accurately predicts the outcome. Movie links for the evolution over time of the collapse are available for the [dispersion](#) [18] and [black hole](#) [19] cases.

We investigate whether this collapse is a Type I or Type II transition [20] by studying the mass of the black hole close to the critical radius. Supposing it is a Type II collapse and let  $R_*$  be the critical point such that  $M_{\text{BH}}(R_*) = 0$ , one can compute the critical index  $\gamma$  defined by

$$M_{\text{BH}} \propto (R - R_*)^\gamma. \quad (11)$$

The value assuming the theoretical prediction of eq. 10,  $R_*^{\text{th}} = \sqrt{1/8\pi\lambda}(G\mu)^{-3/2}M_{\text{Pl}}^{-1}$ , is  $\gamma = 0.39$ , see fig. 3. However, in our simulations we have observed  $R_*^{\text{ob}} > R_*^{\text{th}}$ , giving  $\gamma = 0.17$ , showing that  $\gamma$  is highly dependent on the choice of the actual value of  $R_*$  – of which we are unable to identify with confidence due to the lack of computational resources. Therefore, we conclude that  $\gamma = 0.28 \pm 0.11$ .

In the subcritical limit where  $2GM_{\text{loop}} < \delta$ , the loop unwinds as it collapses, transferring all the mass into matter and gravitational radiation. If  $R \gg \delta$  the velocity at unwinding is much larger than the escape velocity and all the energy is radiated away. However, if  $R \sim \delta$ , the velocity can be small enough so that instead of full dispersal the mass slowly decays at the center and a soliton might form.

#### IV. GRAVITATIONAL WAVES FROM BLACK HOLE FORMATION

We compute the gravitational waveform from the collapse of a loop with  $G\mu = 1.6 \times 10^{-2}$  and  $R = 100 M_{\text{Pl}}^{-1}$  into a black hole, fig. 1. Post formation of the apparent

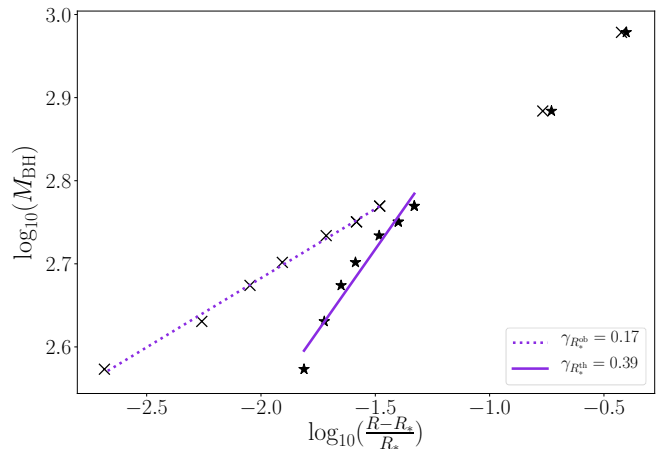


FIG. 3. **Critical collapse**: We plot the logarithm of the mass of the black hole vs the logarithm of the difference between the initial and the theoretical(star)/observed(cross) critical radius for  $G\mu = 1.6 \times 10^{-2}$ . As we argued in the text, our simulation showed that the actual  $R_*^{\text{ob}} > R_*^{\text{th}}$ , resulting in a critical index within  $0.17 < \gamma < 0.39$ , where the error is due to the uncertainty in determining numerically  $R_*^{\text{th}} < R_* < R_*^{\text{ob}}$ . Note that we only use the first 7 points to compute the critical index for  $R \leq 0.05R_*$  as the critical relation is only expected to hold perturbatively.

horizon, the waveform exhibits the characteristic quasi-normal mode decay, with the dominant mode being the  $l = 2, m = 0$  mode as usual. We found the integrated energy of the signal to be

$$\frac{E_{\text{GW}}}{M_{\text{loop}}} = 0.5 \pm 0.2 \%. \quad (12)$$

The error bars come primarily from the presence of the spurious modes from the initial data mixing in with the early part of the collapse (grey area in fig. 1). Even though the velocity of the loop at collision is ultra-relativistic,  $\sim 0.99 c$ , the GW production is strongly suppressed when compared to other ultra-relativistic events. For comparison, a boosted head-on black hole merger ( $14 \pm 3\%$ ) and relativistic fluid particle collapse ( $16 \pm 2\%$ ) radiates a much larger fraction of its total mass in gravitational waves [21, 22]. This suggests that the initial apparent horizon is very spherical – possibly due to the thickness of our strings when compared to the Schwarzschild radius, i.e.  $2GM_{\text{loop}} \sim \mathcal{O}(1) \times \delta$ . In the limit of infinitesimally thin strings, the maximum GW production was calculated by Hawking to be 29% [17]. Hence, we believe that one can boost the efficiency by colliding thinner strings (i.e.  $2GM_{\text{loop}} \gg \delta$ ) – in this limit the hoop conjecture argument above suggests that a black hole will form before the loop has a chance to interact and unwind, thus it is possible that the GW emission will be larger via Hawking’s argument, though this has not been demonstrated numerically.

Finally, loops in general are generated non-circularly

with many different oscillating stable configurations. Nevertheless, in the presence of gravity, we expect gravity to eventually win out, with roughly the timescale of their gravitational collapse to be the free-fall time-scale. In the final stages of collapse, we expect the tension to circularize the loops and thus our results should hold in general.

## V. DISCUSSION AND DETECTION PROSPECTS

We have extracted the gravitational wave signal for the case  $G\mu = 1.6 \times 10^{-2}$ , and  $R = 100 M_{\text{Pl}}^{-1}$  and found that  $0.5 \pm 0.2\%$  of the initial mass is radiated into gravitational waves. The QNM frequency of our GW waveform (fig. 1) is in the UV range and out of any current or future detectors. On the other hand, if we assume that our numerical results scale, we can ask whether we can detect suitably massive cosmic strings loops with current or future detectors. The two key parameters are (i) the frequency and (ii) the luminosity of the event. The frequency band of detectors depend on the masses. For LIGO/VIRGO and the Einstein Telescope, this is  $\sim 100$  Hz, corresponding to  $\sim 100 M_{\odot}$  black holes. This constraints our parameter space to

$$\mu R \approx 16 M_{\odot}, \quad (13)$$

which for the case of  $G\mu \sim 10^{-2}$  considered in this paper, gives  $R \approx 10^3$  km. For more realistic cosmic string tensions bounded by the recent LIGO/VIRGO observations,  $G\mu \leq 10^{-7}$  [3]. Choosing  $G\mu = 10^{-8}$ , we find the loop to be approximately solar system scale  $R \sim 10$  au, with a free fall time of  $\sim \mathcal{O}(10^2)$  yrs).

Meanwhile, the strain  $h$  observed at a distance  $d$  from a source of GWs is

$$\left(\frac{h}{10^{-21}}\right) \sim \sqrt{\frac{E_{\text{GW}}}{3 \times 10^{-3} M_{\odot}}} \left(\frac{10 \text{ Mpc}}{d}\right). \quad (14)$$

From our simulations, we find an efficiency of  $0.5 \pm 0.2\%$ , thus  $E_{\text{GW}} = 5 \times 10^{-3} M_{\text{loop}}$  so for  $100 M_{\odot}$  cosmic string loops  $E_{\text{GW}} \approx 0.5 M_{\odot}$ , resulting in  $d \sim (10^{-19}/h)$  Mpc. Finally, to know the approximate number of solar system sized loops that are expected to be within a radius  $d$  we follow the number densities obtained from different

models. The number of loops scales as

$$N_{\text{loop}} \propto \mathcal{A} \left(\frac{d}{\text{Gpc}}\right)^3, \quad (15)$$

where  $\mathcal{A}$  is a model dependent prefactor which for references [16] and [23] is  $\mathcal{A} = 10^{-3}$  and  $\mathcal{A} = 10^5$  respectively. Translating this to rate of events per year, we obtained

$$\Gamma_{\text{LV}} \approx 0.1 - 10^{-9} \text{ events/yr}, \quad (16)$$

$$\Gamma_{\text{ET}} \approx 100 - 10^{-6} \text{ events/yr}, \quad (17)$$

for LIGO/VIRGO and the Einstein Telescope respectively, whereas similar results of LIGO/VIRGO have been found for LISA.

Hence, in the most optimistic scenario we would detect one black hole formed from a collapsed cosmic string loop every decade or so with LIGO/VIRGO. We emphasise that this is a conservative estimate since these solar system sized loops satisfy  $R_{\text{BH}} \sim \mathcal{O}(10^{37}) \times \delta$  and hence are thin loops. As mentioned before,  $E_{\text{GW}}/M_{\text{loop}}$  might be closer to 29 % as Hawking suggested [17], increasing the rate for LIGO/VIRGO to  $10 - 10^{-7}$  events/yr and the Einstein Telescope  $10^4 - 10^{-4}$  events/yr. We will numerically investigate the collapse of these thin loops in a future work.

## ACKNOWLEDGMENTS

We acknowledge useful conversations with José Juan Blanco-Pillado, Katy Clough, Ed Copeland, William East, Mark Hindmarsh, Paul Shellard, James Widdicombe and Helvi Witek. We would also like to thank the GRChombo team (<http://www.grchombo.org/>) and the COSMOS team at DAMTP, Cambridge University for their ongoing technical support. Special thanks to Federica Albertini, Gregorio Carullo and Alastair Wickens. Numerical simulations were performed on the COSMOS supercomputer and the Cambridge CSD3 HPC, funded by DIRAC3/BIS, on BSC Marenostrum IV via PRACE grant Tier-0 PFPWG, by the Supercomputing Centre of Galicia and La Palma Astrophysics Centre via BSC/RES grants AECT-2017-2-0011 and AECT-2017-3-0009 and on SurfSara Cartesius under Tier-1 PRACE grant DECI-14 14DECI0017.

---

[1] B. P. Abbott *et al.* (Virgo, LIGO Scientific), *Phys. Rev. Lett.* **116**, 061102 (2016), arXiv:1602.03837 [gr-qc].  
 [2] T. W. B. Kibble, *J. Phys.* **A9**, 1387 (1976).  
 [3] B. Abbott *et al.* (Virgo, LIGO Scientific), *Phys. Rev. D* **97**, 102002 (2018), arXiv:1712.01168 [gr-qc].  
 [4] E. J. Copeland and T. W. B. Kibble, *Proc. Roy. Soc. Lond.* **A466**, 623 (2010), arXiv:0911.1345 [hep-th].

[5] L. Pogosian, S. H. H. Tye, I. Wasserman, and M. Wyman, *Phys. Rev. D* **68**, 023506 (2003), [Erratum: *Phys. Rev. D* **73**, 089904 (2006)], arXiv:hep-th/0304188 [hep-th].  
 [6] N. T. Jones, H. Stoica, and S. H. H. Tye, *Phys. Lett. B* **563**, 6 (2003), arXiv:hep-th/0303269 [hep-th].  
 [7] P. A. R. Ade *et al.* (Planck), *Astron. Astrophys.* **571**, A25 (2014), arXiv:1303.5085 [astro-ph.CO].

- [8] A. Vilenkin and E. P. S. Shellard, *Cosmic Strings and Other Topological Defects* (Cambridge University Press, 2000).
- [9] A. Vilenkin, Phys. Lett. **107B**, 47 (1981).
- [10] T. Damour and A. Vilenkin, Phys. Rev. **D71**, 063510 (2005), arXiv:hep-th/0410222 [hep-th].
- [11] M. Hindmarsh, J. Lizarraga, J. Urrestilla, D. Daverio, and M. Kunz, Phys. Rev. **D96**, 023525 (2017), arXiv:1703.06696 [astro-ph.CO].
- [12] G. Vincent, N. D. Antunes, and M. Hindmarsh, Phys. Rev. Lett. **80**, 2277 (1998), arXiv:hep-ph/9708427 [hep-ph].
- [13] J. N. Moore and E. P. S. Shellard, (1998), arXiv:hep-ph/9808336 [hep-ph].
- [14] K. D. Olum and J. J. Blanco-Pillado, Phys. Rev. **D60**, 023503 (1999), arXiv:gr-qc/9812040 [gr-qc].
- [15] J. N. Moore, E. P. S. Shellard, and C. J. A. P. Martins, Phys. Rev. **D65**, 023503 (2002), arXiv:hep-ph/0107171 [hep-ph].
- [16] J. J. Blanco-Pillado, K. D. Olum, and B. Shlaer, Phys. Rev. **D83**, 083514 (2011), arXiv:1101.5173 [astro-ph.CO].
- [17] S. Hawking, Physics Letters B **246**, 36 (1990).
- [18] GRChombo, “Dispersion - cosmic string loop collapse in full gr,” (2018), <https://youtu.be/nHH3gTEjMPo>.
- [19] GRChombo, “Black hole formation - cosmic string loop collapse,” (2018), <https://youtu.be/U5CkThsDU6w>.
- [20] C. Gundlach, Living Rev. Rel. **2**, 4 (1999), arXiv:gr-qc/0001046 [gr-qc].
- [21] U. Sperhake, V. Cardoso, F. Pretorius, E. Berti, and J. A. Gonzalez, Phys. Rev. Lett. **101**, 161101 (2008), arXiv:0806.1738 [gr-qc].
- [22] W. E. East and F. Pretorius, Phys. Rev. Lett. **110**, 101101 (2013), arXiv:1210.0443 [gr-qc].
- [23] C. Ringeval, M. Sakellariadou, and F. Bouchet, JCAP **0702**, 023 (2007), arXiv:astro-ph/0511646 [astro-ph].
- [24] K. Clough, P. Figueras, H. Finkel, M. Kunesch, E. A. Lim, and S. Tunyasuvunakool, Class. Quant. Grav. **32**, 245011 (2015), [Class. Quant. Grav.32,24(2015)], arXiv:1503.03436 [gr-qc].
- [25] T. W. Baumgarte and S. L. Shapiro, Phys. Rev. **D59**, 024007 (1999), arXiv:gr-qc/9810065 [gr-qc].
- [26] M. Shibata and T. Nakamura, Phys. Rev. D **52**, 5428 (1995).
- [27] M. Shibata and T. Nakamura, Phys.Rev. **D52**, 5428 (1995).
- [28] M. Campanelli, C. O. Lousto, P. Marronetti, and Y. Zlochower, Phys. Rev. Lett. **96**, 111101 (2006), arXiv:gr-qc/0511048 [gr-qc].
- [29] J. G. Baker, J. Centrella, D.-I. Choi, M. Koppitz, and J. van Meter, Phys. Rev. Lett. **96**, 111102 (2006), arXiv:gr-qc/0511103 [gr-qc].
- [30] M. Zilhó, H. Witek, and V. Cardoso, Class. Quant. Grav. **32**, 234003 (2015), arXiv:1505.00797 [gr-qc].
- [31] D. Hilditch, *Proceedings, Spring School on Numerical Relativity and High Energy Physics (NR/HEP2): Lisbon, Portugal, March 11-14, 2013*, Int. J. Mod. Phys. **A28**, 1340015 (2013), arXiv:1309.2012 [gr-qc].
- [32] C. Palenzuela, L. Lehner, and S. Yoshida, Phys. Rev. **D81**, 084007 (2010), arXiv:0911.3889 [gr-qc].
- [33] J. G. Baker, M. Campanelli, and C. O. Lousto, Phys. Rev. **D65**, 044001 (2002), arXiv:gr-qc/0104063 [gr-qc].
- [34] K. D. Kokkotas and B. G. Schmidt, Living Reviews in Relativity **2**, 2 (1999).
- [35] M. Nagasawa and J. Yokoyama, Phys. Lett. **B345**, 416 (1995), arXiv:astro-ph/9404041 [astro-ph].

## Appendix A: Numerical Methodology

### 1. Evolution Equations

In this work, we use GRCHOMBO, a multipurpose numerical relativity code [24] which solves the BSSN [25–27] formulation of the Einstein equation. The 4 dimensional spacetime metric is decomposed into a spatial metric on a 3 dimensional spatial hypersurface,  $\gamma_{ij}$ , and an extrinsic curvature  $K_{ij}$ , which are both evolved along a chosen local time coordinate  $t$ . The line element of the decomposition is

$$ds^2 = -\alpha^2 dt^2 + \gamma_{ij}(dx^i + \beta^i dt)(dx^j + \beta^j dt) , \quad (\text{A1})$$

where  $\alpha$  and  $\beta^i$  are the lapse and shift, gauge parameters. These gauge parameters are specified on the initial hypersurface and then allowed to evolve using gauge-driver equations, in accordance with the puncture gauge [28, 29], for which the evolution equations are

$$\partial_t \alpha = -\mu \alpha K + \beta^i \partial_i \alpha , \quad (\text{A2})$$

$$\partial_t \beta^i = B^i , \quad (\text{A3})$$

$$\partial_t B^i = \frac{3}{4} \partial_t \Gamma^i - \eta B^i , \quad (\text{A4})$$

where the constants  $\eta$  and  $\mu$  are of order  $1/M_{\text{ADM}}$  and unity respectively.

The induced metric is decomposed as

$$\gamma_{ij} = \frac{1}{\chi} \tilde{\gamma}_{ij} , \quad \det \tilde{\gamma}_{ij} = 1 , \quad \chi = (\det \gamma_{ij})^{-\frac{1}{3}} . \quad (\text{A5})$$

The extrinsic curvature is decomposed into its trace,  $K = \gamma^{ij} K_{ij}$ , and its traceless part  $\tilde{\gamma}^{ij} \tilde{A}_{ij} = 0$  as

$$K_{ij} = \frac{1}{\chi} \left( \tilde{A}_{ij} + \frac{1}{3} K \tilde{\gamma}_{ij} \right) . \quad (\text{A6})$$

The conformal connections are  $\tilde{\Gamma}^i = \tilde{\gamma}^{jk} \tilde{\Gamma}_{jk}^i$  where  $\tilde{\Gamma}_{jk}^i$  are the Christoffel symbols associated with the conformal metric  $\tilde{\gamma}_{ij}$ . The evolution equations for the gravity sector

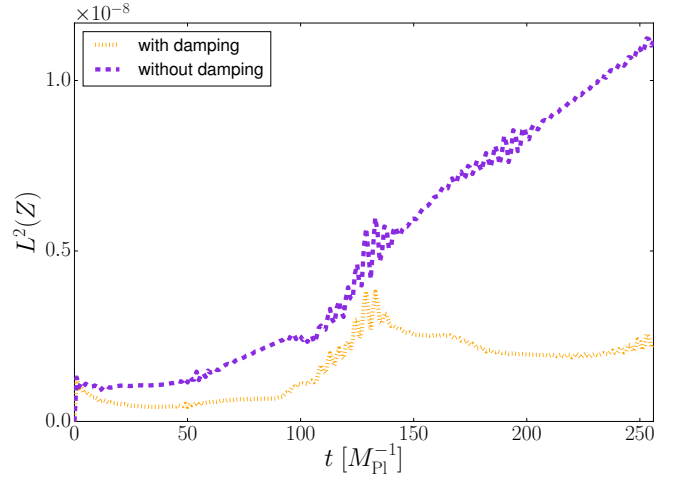


FIG. 4. **Gauss constraint for static string:** We run the same simulation for an infinite static string with  $G\mu = 1.6 \times 10^{-2}$  ( $\eta = 0.05 M_{\text{Pl}}$ ) with and without damping. We find that the damping stabilises the linear growth in violation.

of BSSN are then

$$\partial_t \chi = \frac{2}{3} \chi \alpha K - \frac{2}{3} \chi \partial_k \beta^k + \beta^k \partial_k \chi , \quad (\text{A7})$$

$$\begin{aligned} \partial_t \tilde{\gamma}_{ij} = & -2 \alpha \tilde{A}_{ij} + \tilde{\gamma}_{ik} \partial_j \beta^k + \tilde{\gamma}_{jk} \partial_i \beta^k \\ & - \frac{2}{3} \tilde{\gamma}_{ij} \partial_k \beta^k + \beta^k \partial_k \tilde{\gamma}_{ij} , \end{aligned} \quad (\text{A8})$$

$$\begin{aligned} \partial_t K = & -\gamma^{ij} D_i D_j \alpha + \alpha \left( \tilde{A}_{ij} \tilde{A}^{ij} + \frac{1}{3} K^2 \right) \\ & + \beta^i \partial_i K + 4\pi \alpha (\rho + S) , \end{aligned} \quad (\text{A9})$$

$$\begin{aligned} \partial_t \tilde{A}_{ij} = & \chi \left[ -D_i D_j \alpha + \alpha (R_{ij} - 8\pi \alpha S_{ij}) \right]^{\text{TF}} \\ & + \alpha (K \tilde{A}_{ij} - 2 \tilde{A}_{il} \tilde{A}^l_j) \\ & + \tilde{A}_{ik} \partial_j \beta^k + \tilde{A}_{jk} \partial_i \beta^k \\ & - \frac{2}{3} \tilde{A}_{ij} \partial_k \beta^k + \beta^k \partial_k \tilde{A}_{ij} , \end{aligned} \quad (\text{A10})$$

$$\begin{aligned} \partial_t \tilde{\Gamma}^i = & 2 \alpha \left( \tilde{\Gamma}_{jk}^i \tilde{A}^{jk} - \frac{2}{3} \tilde{\gamma}^{ij} \partial_j K - \frac{3}{2} \tilde{A}^{ij} \frac{\partial_j \chi}{\chi} \right) \\ & - 2 \tilde{A}^{ij} \partial_j \alpha + \beta^k \partial_k \tilde{\Gamma}^i \\ & + \tilde{\gamma}^{jk} \partial_j \partial_k \beta^i + \frac{1}{3} \tilde{\gamma}^{ij} \partial_j \partial_k \beta^k \\ & + \frac{2}{3} \tilde{\Gamma}^i \partial_k \beta^k - \tilde{\Gamma}^k \partial_k \beta^i - 16\pi \alpha \tilde{\gamma}^{ij} S_j . \end{aligned} \quad (\text{A11})$$

Meanwhile, the matter part of the Lagrangian is

$$\mathcal{L}_m = -(D_\mu \phi)^* (D^\mu \phi) - \frac{1}{4} F_{\mu\nu} F^{\mu\nu} - V(\phi) , \quad (\text{A12})$$

which gives the evolution equations

$$-D_\mu D^\mu \phi + \frac{\partial V(\phi)}{\partial \bar{\phi}} = 0 , \quad (\text{A13})$$

$$\nabla_\mu F^{\mu\nu} = -e J^\nu , \quad (\text{A14})$$

with

$$J^\nu = 2\text{Im}(\phi^* D^\nu \phi) , \quad F_{\mu\nu} = \partial_\mu A_\nu - \partial_\nu A_\mu . \quad (\text{A15})$$

We decompose these equations in 3+1 coordinates, following [30]. Furthermore, we impose the Lorenz condition

$$\nabla^\mu A_\mu = 0 . \quad (\text{A16})$$

Using the projector

$$P_\mu^\nu = \delta_\mu^\nu + n_\mu n^\nu , \quad (\text{A17})$$

where  $n^\mu$  is the normal to the hypersurface, the gauge field and current can further be decomposed into transverse and longitudinal components via

$$\begin{aligned} A_\mu &= \mathcal{A}_\mu + n_\mu \mathcal{A} , \\ J_\mu &= \mathcal{J}_\mu + n_\mu \mathcal{J} , \end{aligned} \quad (\text{A18})$$

such that

$$\begin{aligned} \mathcal{A}_\mu &= P_\mu^\nu A_\nu \quad \text{and} \quad \mathcal{A} = -n^\nu A_\nu , \\ \mathcal{J}_\mu &= P_\mu^\nu J_\nu \quad \text{and} \quad \mathcal{J} = -n^\nu J_\nu . \end{aligned} \quad (\text{A19})$$

The electric and magnetic fields are defined as

$$E_\mu = P_\mu^\nu n^\rho F_{\nu\rho} , \quad (\text{A20})$$

$$B_\mu = P_\mu^\nu n^\rho (\star F_{\nu\rho}) , \quad (\text{A21})$$

where  $(\star F_{\nu\rho})$  is the dual Maxwell tensor. Using the previous decomposition we rewrite the Maxwell tensor as

$$F_{\mu\nu} = n_\mu E_\nu - n_\nu E_\mu + \partial_\mu \mathcal{A}_\nu - \partial_\nu \mathcal{A}_\mu . \quad (\text{A22})$$

In addition, eq. A14 gives the Gauss constraint

$$\tilde{\nabla}_i E^i = -e\mathcal{J} , \quad (\text{A23})$$

where  $\tilde{\nabla} = P_\mu^\nu \nabla_\nu$ .

To ensure that numerical violation of eq. A23 is kept to a minimum, we stabilise it by introducing an auxiliary damping variable  $Z$  [30–32], resulting in the following modified evolution equations

$$\begin{aligned} \partial_t E^i &= \alpha(E_i - e\mathcal{J}^i + \tilde{\nabla}_i \mathcal{A}) - \mathcal{A} \tilde{\nabla}_i \alpha + \beta^j \partial_j E^i \\ &\quad - E^j \partial_j \beta^i , \end{aligned} \quad (\text{A24})$$

$$\partial_t \mathcal{A} = -\mathcal{A}^i \tilde{\nabla}_i \alpha + \alpha(K\mathcal{A} - \tilde{\nabla}_i \mathcal{A}^i - Z) + \beta^j \partial_j \mathcal{A} , \quad (\text{A25})$$

$$\begin{aligned} \partial_t \mathcal{A}_i &= -\alpha(E_i + \tilde{\nabla}_i \mathcal{A}) - \mathcal{A} \tilde{\nabla}_i \alpha + \beta^j \partial_j \mathcal{A}_i \\ &\quad + \partial_i \beta^j \mathcal{A}_j , \end{aligned} \quad (\text{A26})$$

$$\partial_t Z = \alpha(\tilde{\nabla}_i E^i - e\mathcal{J} - \kappa Z) + \beta^j \partial_j Z . \quad (\text{A27})$$

From fig. 4 we see the scheme is effective at stopping the growth of constraint violations.

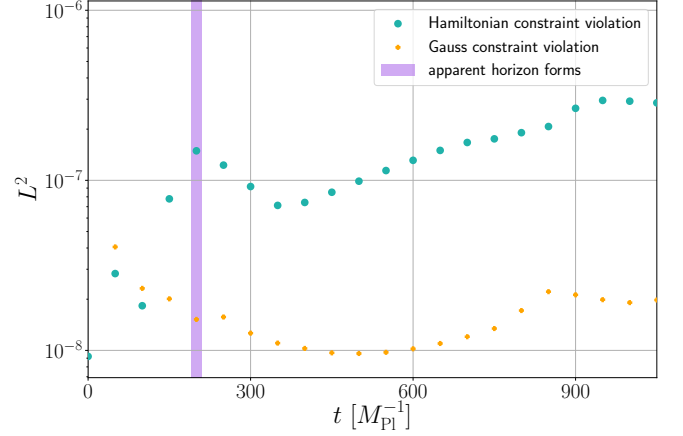


FIG. 5.  **$L^2$  norm of constraints:** Loop with  $G\mu = 1.6 \times 10^{-2}$  and  $R = 100 M_{\text{Pl}}^{-1}$  remains stable throughout evolution, even after black hole formation. The initial Hamiltonian constraint is smaller than it can be maintained by the evolution scheme. The momentum constraints violation are negligible throughout.

Finally, we decompose the complex scalar field

$$\phi = \frac{1}{\sqrt{2}} (\phi_1 + i\phi_2) , \quad (\text{A28})$$

and rewriting the matter equation with BSSN variables,

$$\partial_t \phi_a = \alpha \Pi_{M,a} + \beta^i \partial_i \phi_a , \quad (\text{A29})$$

$$\begin{aligned} \partial_t \Pi_{M,a} &= \beta^i \partial_i \Pi_{M,a} + \alpha \partial_i \partial^i \phi_a + \partial_i \phi_a \partial^i \alpha \\ &\quad + \alpha \left( K \Pi_{M,a} - \gamma^{ij} \Gamma_{ij}^k \partial_k \phi_a + \frac{dV}{d\phi_a} \right) \\ &\quad + \alpha (-e^2 A_\mu A^\mu \phi_a \pm e \phi_{a+1} \nabla_\mu A^\mu \\ &\quad \pm 2e A^\mu \partial_\mu \phi_{a+1}) , \end{aligned} \quad (\text{A30})$$

$$\begin{aligned} \partial_t E^i &= \alpha K E^i + e \alpha \chi \tilde{\gamma}^{ij} \mathcal{J}_j + \alpha \chi \tilde{\gamma}^{ij} \partial_j Z \\ &\quad + \chi^2 \tilde{\gamma}^{ij} \tilde{\gamma}^{kl} \partial_l \alpha (\partial_j \mathcal{A}_k - \partial_k \mathcal{A}_j) \\ &\quad + \chi^2 \tilde{\gamma}^{ij} \tilde{\gamma}^{kl} (\tilde{D}_k \partial_j \mathcal{A}_l - \tilde{D}_k \partial_l \mathcal{A}_j) \\ &\quad + \frac{\alpha}{2} \chi \tilde{\gamma}^{ij} \tilde{\gamma}^{kl} (\partial_j \mathcal{A}_l \partial_k \chi - \partial_k \mathcal{A}_j \partial_l \chi) \\ &\quad + \beta^j \partial_j E^i - E^j \partial_j \beta^i - \alpha e \mathcal{J}^i , \end{aligned} \quad (\text{A31})$$

$$\begin{aligned} \partial_t \mathcal{A} &= \alpha K \mathcal{A} - \alpha \chi \tilde{\gamma}^{ij} \partial_j \mathcal{A}_i + \alpha \chi \mathcal{A}_i \tilde{\Gamma}^i - \alpha Z \\ &\quad + \frac{\alpha}{2} \mathcal{A}_i \tilde{\gamma}^{ij} \partial_j \chi - \chi \tilde{\gamma}^{ij} \mathcal{A}_i \partial_j \alpha + \beta^j \partial_j \mathcal{A} , \end{aligned} \quad (\text{A32})$$

$$\begin{aligned} \partial_t \mathcal{A}_i &= -\alpha \chi^{-1} \tilde{\gamma}_{ij} E^j - \alpha \partial_i \mathcal{A} - \mathcal{A} \partial_i \alpha \\ &\quad + \beta^j \partial_j \mathcal{A}_i + \partial_i \beta^j \mathcal{A}_j , \end{aligned} \quad (\text{A33})$$

$$\partial_t Z = \alpha \tilde{\nabla}_i E^i - \frac{3}{2} \frac{\alpha}{\chi} E^i \partial_i \chi - \alpha e \mathcal{J} - \alpha \kappa Z + \beta^j \partial_j Z , \quad (\text{A34})$$

where  $a \in \{1, 2\}$  and the second order Klein Gordon equation has been decomposed into two first order equations as usual. The stress energy tensor for Abelian-Higgs

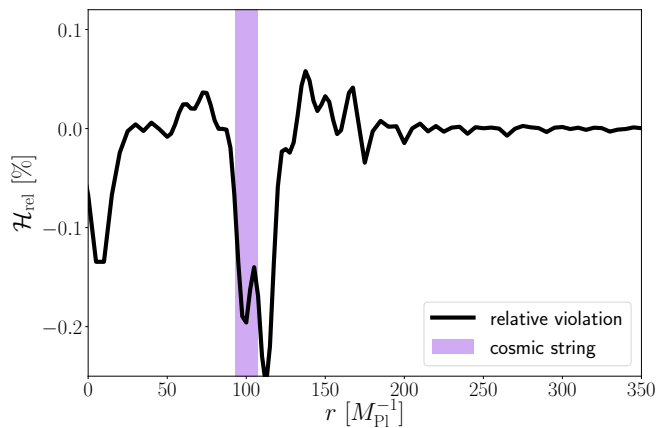


FIG. 6. **Initial relative violation:** Slice through initial data for loop from center through string with  $G\mu = 1.6 \times 10^{-2}$  and initial radius  $R = 100 M_{\text{Pl}}^{-1}$ . The green region indicates where the string is located. We find that there is an error of at most 0.3%.

is

$$T_{\mu\nu} = D_{(\mu}\phi^* D_{\nu)}\phi + F_{\mu\alpha}F_{\nu}^{\alpha} + g_{\mu\nu}\mathcal{L}_m, \quad (\text{A35})$$

and its various components are defined as

$$\begin{aligned} \rho &= n_a n_b T^{ab}, & S_i &= -\gamma_{ia} n_b T^{ab}, \\ S_{ij} &= \gamma_{ia} \gamma_{jb} T^{ab}, & S &= \gamma^{ij} S_{ij}. \end{aligned} \quad (\text{A36})$$

The Hamiltonian constraint

$$\mathcal{H} = R + K^2 - K_{ij}K^{ij} - 16\pi\rho, \quad (\text{A37})$$

the momentum constraint

$$\mathcal{M}_i = D^j(\gamma_{ij}K - K_{ij}) - 8\pi S_i, \quad (\text{A38})$$

and the Gauss constraint

$$\mathcal{Z} = \tilde{\nabla}_i E^i - e\mathcal{J}^\nu n_\nu, \quad (\text{A39})$$

are monitored throughout the evolution to check the quality of our simulations (see fig. 5). Our boundary conditions are Dirichlet.

## 2. Initial Data

We set up the field as mentioned in the main text using toroidal coordinates (see fig. 7). Time symmetry is assumed for our initial data,

$$K = 0, \quad A_{ij} = 0, \quad (\text{A40})$$

which automatically fulfils the momentum constraint (eq. A38). In addition, we make a conformally flat ansatz  $\tilde{\gamma}_{ij}$ ,

$$\tilde{\gamma}_{ij} = \delta_{ij}, \quad (\text{A41})$$

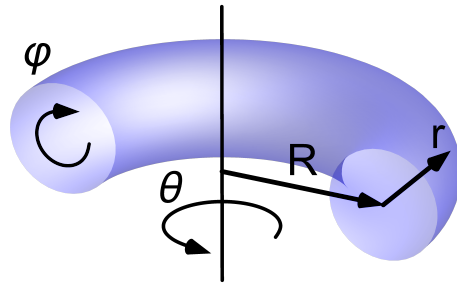


FIG. 7. **Toroidal coordinates** encode the symmetry of our cosmic string loops. They are used to generate the initial field configuration, where  $R$  defines the radius of the loop.

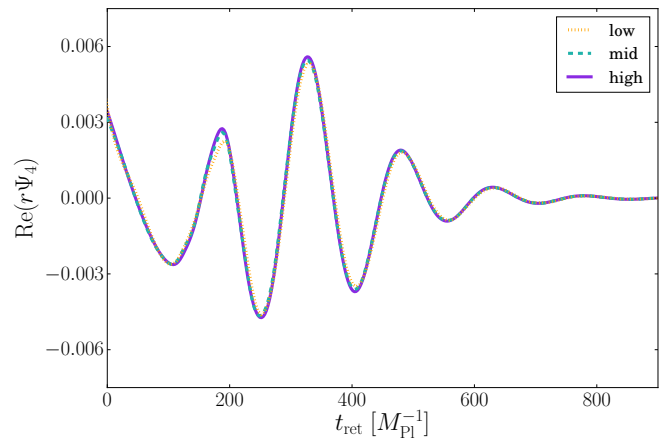


FIG. 8. **Convergence in  $r\Psi_4$**  between low, mid and high resolutions giving an overall 2nd-3rd order convergence. The x-axis  $t_{\text{ret}} = t - r_{\text{ext}}$  is the retarded time where  $r_{\text{ext}}$  is the extraction radius.

and impose the metric to be identity in the center of the string, similar as the static string (see eq. B5). We find that doing so reduces possible excitations of the string. For the gravitational wave extraction, we impose the condition

$$\lim_{r \rightarrow \infty} \chi = 1. \quad (\text{A42})$$

We solve for  $\chi$  using the Hamiltonian constraint eq. A37. We reduce the spatial dimension of the problem by using its cylindrical symmetry. This solution is then further relaxed to obtain the final solution, which is that of an excited cosmic string loop.

As shown in fig. 6, the relative Hamiltonian violation



from our prescription is

$$\mathcal{H}_{\text{rel}} = \frac{\mathcal{H}}{16\pi\rho_{\text{max}}} < 1\% .$$

### 3. Numerical Extraction of Signal

We extract the Penrose scalar  $\Psi_4$  with tetrads proposed by [33]. Similarly as in black hole binaries, there is some non-physical radiation associated with the initial data, which in our case consists of a toroidal shell of artificial radiation resulting in two GW peaks before the physical signal. While such stray-GW can often be ignored as they quickly radiate away at light speed, in our case due to the rapid collapse of our loops at ultra-relativistic speeds, they cannot be ignored.

The first peak at  $t_{\text{ret}} < 0$  is due to this initial radiation travelling opposite to the collapse and could be separated by increasing the loop radius so that the real signal takes longer. However, the second peak (first peak in fig. 1) results from the radiation which travels together with the collapsing loop at similar velocity, which always mixes with the real signal. In any case, increasing the loop radius would result in a cleaner signal but this is computationally very expensive.

To estimate the GW energy we use the equation

$$\frac{dE_{\text{GW}}}{dt} = \frac{r^2}{16\pi} \int_{\mathcal{S}_r} \left| \int_{t_0}^t \Psi_4 dt' \right|^2 d\Omega , \quad (\text{A43})$$

where  $\mathcal{S}_r$  is a sphere of radius  $r$ .

In the cases for which the cosmic string loop does not form a black hole, most of the matter will escape, typically at velocities close to the speed of light. This scalar and vector radiation overlaps the gravitational wave signal and due to its large mass might leave an imprint on  $r\Psi_4$ , making the signal extraction problematic<sup>3</sup>.

### 4. Numerics and Convergence Tests

In fig. 5, we show that the volume-averaged Hamiltonian constraint violation

$$L^2(H) = \sqrt{\frac{1}{V} \int_V |\mathcal{H}^2| dV} , \quad (\text{A44})$$

where  $V$  is the box volume with the interior of the apparent horizon excised, is under control throughout the simulation.

We use the gradient conditions on  $\phi$  and  $\chi$  to tag cells for regridding. The precise criteria is chosen depending

<sup>3</sup> This could be prevented by setting the extraction zone further out, but this is numerically too expensive.

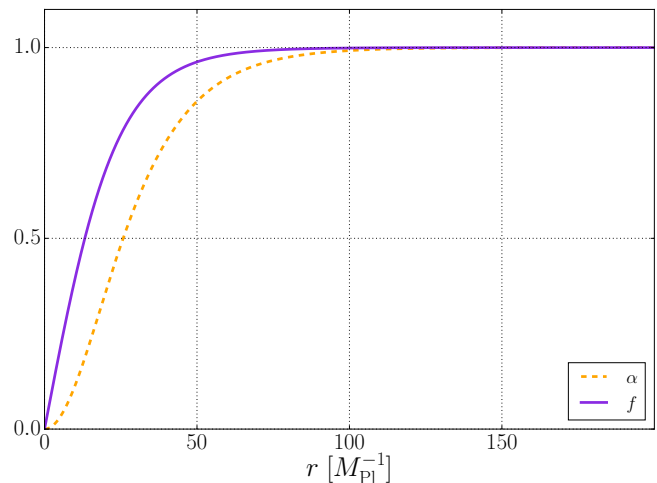


FIG. 9. **Radial profile of  $\alpha$  and  $f$**  for an infinite static string with gravity in the critical coupling limit ( $e = 1$ ,  $\lambda = 2$ ) and  $\eta = 0.05 M_{\text{Pl}}$  ( $G\mu = 1.6 \times 10^{-2}$ ).

on the symmetry breaking scale  $\eta$  and the total mass of the system. The major distinction for the amount of resolution needed is whether GW are being extracted or not. To obtain a clean GW large boxes are needed to avoid the detection of reflections of the non-physical signal with the boundaries, which increases the cost of the simulation. We double checked that our signal in fig. 1 was consistent with a  $l = 2$   $m = 0$  QNM [34] within numerical error.

We tested the convergence of our simulations with a cosmic string loop of  $\eta = 0.05$  ( $G\mu = 1.6 \times 10^{-2}$ ) and  $R = 100 M_{\text{Pl}}^{-1}$  by using a box of size  $L = 2048 M_{\text{Pl}}^{-1}$  in which we improved by a factor of 1.5 between all three resolutions. The convergence of  $r\Psi_4$  for low ( $\Delta x_{\text{min}} = 1.33 M_{\text{Pl}}^{-1}$ ), medium ( $\Delta x_{\text{min}} = 1.00 M_{\text{Pl}}^{-1}$ ) and high ( $\Delta x_{\text{min}} = 0.66 M_{\text{Pl}}^{-1}$ ) resolutions is shown in fig. 8.

### Appendix B: Abelian-Higgs Code Test

To test the code, we compare the evolution of a simulation with a known semi-analytic case of the infinite static string [8]. Given the symmetry of the problem we use polar coordinates

$$\begin{aligned} x &= r \cos(\theta) , \\ y &= r \sin(\theta) , \\ z &= z . \end{aligned} \quad (\text{B1})$$

and choose cylindrically symmetric ansatz for the scalar and gauge fields  $\phi$  and  $A_\mu$

$$\begin{aligned} \phi &= f(r)e^{in\theta} , \\ A_\theta &= \frac{n\alpha(r)}{e} , \end{aligned} \quad (\text{B2})$$

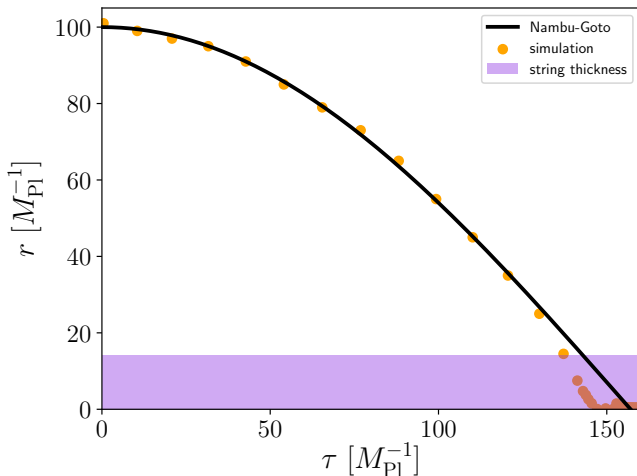


FIG. 10. **Comparison with Nambu-Goto** for loop with  $G\mu = 1.6 \times 10^{-2}$  and initial radius  $R = 100 M_{\text{Pl}}^{-1}$  shows agreement.

and all other components are set to zero. We impose the boundary conditions

$$\begin{aligned} f(0) &= 0, & f(\infty) &= 1, \\ \alpha(0) &= 0, & \alpha(\infty) &= 1. \end{aligned} \quad (\text{B3})$$

For the metric, the following ansatz is chosen

$$ds^2 = -e^{A(r)} dt^2 + e^{B(r)} (dr^2 + r^2 d\theta^2) + e^{A(r)} dz^2, \quad (\text{B4})$$

where  $A(r)$  and  $B(r)$  are radial functions numerically determined. We impose the metric and its derivatives to be locally flat

$$\begin{aligned} A(0) &= 0, & A'(0) &= 0, \\ B(0) &= 0, & B'(0) &= 0. \end{aligned} \quad (\text{B5})$$

We solve Einstein's and the corresponding matter evolution equations

$$G_{\mu\nu} = 8\pi T_{\mu\nu}, \quad (\text{B6})$$

$$D_\mu D^\mu \phi = \frac{dV}{d\phi}, \quad (\text{B7})$$

iteratively as follows. We solve the Klein-Gordon equation (eq. B7) for fixed flat background, then use this solution to calculate the stress-energy tensor and retrieve the values of  $A(r)$  and  $B(r)$  via (B6) to build a new metric. Plugging this back into the Klein-Gordon equation we find new profiles for the fields using the new metric as background. The solution converges quickly (within  $\sim 5$  iterations), see fig. 9 for the obtained profiles of  $f$  and  $\alpha$ .

### Appendix C: Comparison with Nambu-Goto

Previous work showed that without gravity [35] the Nambu-Goto (NG) action is still valid at relativistic speeds. However, a comparison between the two approaches, leads to consistent results with NG up to roughly the point when the string radius is close to the string thickness (see fig. 10). To reduce gauge effects we use the time of static observer at the position of the string,

$$\tau = \int \alpha|_{\rho=\max(\rho)} dt. \quad (\text{C1})$$

Having shown that NG is a good approximation, we use it to estimate the velocity before unwinding, which we define as the point where the radius of the ring  $R$  is equal to the thickness of the string  $\delta$ . We find

$$v_\delta = \sqrt{1 - \left(\frac{\delta}{R}\right)^2}, \quad (\text{C2})$$

which, for our simulations, gives results ranging from  $0.97 c$  to  $0.99 c$ . In the case for which we extract the gravitational wave signal ( $G\mu = 1.6 \times 10^{-2}$ ,  $R = 100 M_{\text{Pl}}^{-1}$ ) we estimate a velocity of  $0.99 c$  before collision.